Article

Autonecrotic Tomato (*Solanum lycopersicum* L.) Line as a Potential Model for Applications in Proximal Sensing of Biotic and Abiotic Stress

Enrico Santangelo [ID], Angelo Del Giudice, Simone Figorilli [ID], Simona Violino [ID], Corrado Costa [ID], Marco Bascietto [ID], Simone Bergonzoli *[ID] and Claudio Beni [ID]

Consiglio per la Ricerca in Agricoltura e l'Analisi dell'Economia Agraria (CREA), Centro di Ricerca Ingegneria e Trasformazioni Agroalimentari, CREA-IT, via della Pascolare 16, 00015 Monterotondo, Italy; enrico.santangelo@crea.gov.it (E.S.); angelo.delgiudice@crea.gov.it (A.D.G.); simone.figorilli@crea.gov.it (S.F.); simona.violino@crea.gov.it (S.V.); corrado.costa@crea.gov.it (C.C.); marco.bascietto@crea.gov.it (M.B.); claudio.beni@crea.gov.it (C.B.)
* Correspondence: simone.bergonzoli@crea.gov.it

Abstract: The autonecrotic tomato line V20368 (working code IGSV) spontaneously develops necrotic lesions with acropetal progression in response to an increase in temperature and light irradiation. The process is associated with the interaction between tomato and *Cladosporium fulvum*, the fungal agent of leaf mold. The contemporary presence of an in-house allele encoding the $Rcr3^{lyc}$ protein and the resistance gene Cf-2^{pim} (from *Solanum pimpinellifolium*) causes auto-necrosis on the leaves even in the absence of the pathogen (hybrid necrosis). The aim of the work was (i) to examine the potential value of the necrotic genotype as a model system for setting up theoretical guidance for monitoring the phytosanitary status of tomato plants and (ii) to develop a predictive model for the early detection of pathogens (or other stresses) in the tomato or other species. Eighteen IGSV tomato individuals at the 4–5th true-leaf stage were grown in three rows (six plants per row) considered to be replicates. The healthy control was the F1 hybrid Elisir (Olter). A second mutant line (SA410) deriving from a cross between the necrotic mutant and a mutant line of the *lutescent* (*l*) gene was used during foliar analysis via microspectrometry. The leaves of the mutants and normal plants were monitored through a portable VIS/NIR spectrometer SCIO™ (Consumer Physics, Tel Aviv, Israel) covering a spectral range between 740 and 1070 nm. Two months after the transplant, the acropetal progression of the autonecrosis showed three symptomatic areas (basal, median, apical) on each IGSV plant: necrotic, partially damaged, and green, respectively. Significantly lower chlorophyll content was found in the basal and median areas of IGSV compared with the control (Elisir). A supervised classification/modelling method (SIMCA) was used. Applying the SIMCA model to the dataset of 162 tomato samples led to the identification of the boundary between the healthy and damaged samples (translational critical distance). Two 10 nm wavelength ranges centred at 865 nm and 1055 nm exhibited a stronger link between symptomatology and spectral reflectance. Studies on specific highly informative mutants of the type described may allow for the development of predictive models for the early detection of pathogens (or other stresses) via proximal sensing.

Keywords: hybrid necrosis; hyperspectral imaging; precision farming; phenotyping

1. Introduction

Plant-pathogen interaction is a complex phenomenon that involves several biochemical gene-driven signalling events [1–3]. In the last few decades, the picture has gradually become clearer thanks to the availability of high-throughput technologies allowing for large amounts of information to be gained [4,5]. One of the main outcomes concerned the plant's ability to recognise extracellular and intracellular pathogens within a general plant immune system [6,7].

In the tomato/*Cladosporium fulvum* (the fungal agent of leaf mold) system, the presence of the resistance gene *Cf-2* confers on the cell the capacity to recognise the avirulence protein delivered by the pathogen, leading to the triggering of a defense cascade [8]. This recognition is made possible by the interaction among three players: the specific protein of the *Cf-2* resistance gene, the proteic ligand of the pathogen (Avr2), and a third cysteine protease coded by the *Rcr3* tomato gene [8,9]. The interaction between Avr2 and Rcr3 is recognised by Cf-2 protein as the signal to turn on the hypersensitive response (HR) and immunity to *C. fulvum* [10].

The resistance gene *Cf-2* and the companion *Rcr3* gene were introduced from the wild species *Solanum pimpinellifolium* [11]. In the cultivated tomato (*Solanum lycopersicum* L.), the contemporary presence of the in-house allele encoding the $Rcr3^{lyc}$ protein and the resistance gene $Cf\text{-}2^{pim}$ causes auto-necrosis (that is, cell death spots) on the leaves even in the absence of the pathogen [9–12]. This uncontrolled cell death is triggered by a form of genetic incompatibility called "hybrid necrosis" leading to phenotypic injuries caused by biotic or abiotic stress even if the stress is absent [12,13]. Another type of "variant" shows an unregulated cell death formation on the leaves resembling a pathogen attack. These lesion-mimic mutants (LMM) present a mutation of specific in-house genes, and in the last 30 years, many mutants have been identified, described, and had their putative underlying mechanisms characterised [14,15]. All these variants and mutants have proven to be useful tools for dissecting the molecular, biochemical, and genetic pathways underlying mainly programmed cell death (PCD) and pathogen resistance pathways in plants [14]. However, hybrid necrosis and LMMs may reveal an instrumental tool for improving the knowledge of plant behaviour in proximal sensing. Early detection is one of the key factors in the successful implementation of optical imaging [16] and the availability of a well-defined plant disease-like system can be used as a model for studying the early diagnosis of diseases from the perspective of its application to precision farming or phenotyping.

In precision agriculture, imaging technologies have been gradually extended from fertilization to the analysis of the sources of intra-field variation, including plant diseases [17–20]. A key turning point in disease sensing concerns the accurate estimation of both the occurrence and severity, coupled with the monitoring of their spreading [21].

Among the available methodologies, those involving hyperspectral imaging in wavelengths of the visible (VIS) range of the spectrum (400–700 nm), near-infrared (NIR) range (700–100 nm), and shortwave infrared (SWIR) range (1000–2500 nm) are the most used for monitoring plant diseases [21,22].

Changes in the plant reflectance pattern caused by pathogenesis may be revealed by studying the variation of hyperspectral data and can allow for the timely detection of disease outbreaks and dynamics [17,23]. Zhang et al. [24] analysed the capacity of hyperspectral remote sensing for detecting late blight in tomatoes, observing the intervals of 750–930 nm and 950–1030 nm to be the best wavelengths for the remote sensing of the disease. Studying the reaction of grapevine genotypes to *Plasmopara viticola*, [25] reveals that the differences in NIR were related to the diversity of the leaf anatomy but also that spectral signatures allowed for differentiation between different symptomatologies of the disease. The same observation about the utility of the spectral signature in differentiating the effect of a foliar pathogen was reported by [26] for the wheat stripe rust, caused by *Puccinia striiformis* f. sp. *tritici*: the reflectance of the infected leaves was higher compared with the corresponding healthy ones, and the difference increased in the days post-inoculation. Some references to the use of hyperspectral imaging in plant/pathogen interactions are reported in Table 1. Data on the potentialities of the VIS/NIR approach in monitoring plant disease are increasing and the reader can find elsewhere a scholarly update [21,23].

Table 1. Review of works involving the use of VIS-NIR and NIR.

#.	Plant Disease	Technique	References
1	Biocontrol of *Trichoderma* spp. by estimating disease severity in young small leafy vegetable plants during specific plant-pathogen-antagonist interactions	VIS-NIR spectroscopy and machine learning	[18]
2	Late blight caused by *Phytophthora infestans* in potato production	Visible/near-infrared (VIS/NIR) spectroscopy with machine learning (ML) and chemometric methods	[27]
3	Early disease in blueberries	Hyperspectral imaging between the spectral range of 400–1000 nm	[28]
4	Anthracnose and gray in the strawberries	Hyperspectral imaging between the spectral range of 400–1000 nm	[29]
5	Fungal infection in citrus fruit	VIS-NIR spectroscopy with range between 325–1100 nm	[30]
6	Anthracnose of banana caused by *Colletotrichum* species	VIS-NIR spectroscopy	[31]
7	Fire blight (FB) of pear trees	Visible-NIR spectrometry method	[32]
8	Gray mold disease caused by *Botrytis cinerea* in tomato	VIS-NIR spectroscopy with range between 550–1100 nm	[33]
9	Micotoxigenic fungi and their toxic metabolites produced in naturally and artificially contaminated products in maize	NIR spectroscopy	[34]
10	Tomato chlorosis virus (ToCV)	VIS-NIR in healthy and diseased leaves at a pre-symptomatic stage	[35]
11	Abiotic and biotic stresses in wild rocket (*Diplotaxis tenuifolia*)	ANN coupled with VIS-NIR and NIR	[19]

The tomato autonecrotic mutant line V20368 (working code IGSV) spontaneously develops necrotic lesions in the acropetal sense at the 5–6th true leaf stage in response to the natural increase in air temperature and light irradiation that occurs during plant growth [36]. The molecular basis involves the interaction between the protein product of the resistance gene *Cf-2^{pim}* and the protease inhibitor encoded by *Rcr3^{lyc}* (hybrid necrosis).

The present work is the first step in describing the leaf phenotype of IGSV. The morphological description of this mutant is deemed to achieve the second objective of outlining its potential in hyperspectral proximal sensing in crop disease detection before and during the appearance of visible symptoms. To this aim, the leaves of necrotic and normal plants have been subjected to a first assessment through a portable VIS/NIR microspectrometer.

To distinguish diseased plants from healthy ones, spectral data were used to approach a statistical method of the supervised classification of data, namely soft independent modelling by class analogy (SIMCA) analysis. SIMCA is a classification and class-modelling method that is based on calculating a PCA model for each class known a priori and choosing an appropriate number of principal components to be used in prediction and quality assessment. This classification method, in contrast with other approaches such as machine learning, allows for classification even on a single class and eliminates the case where an unknown object does not belong to any of the classes considered. In fact, with a discriminant-type approach, it would be incorrectly assigned to one of the classes. SIMCA is used to eliminate this type of error. Thus, a law is considered that does not discriminate between a number of classes, but between membership and non-membership; this is made possible by building a model for each class and using it to determine whether an unknown object belongs to the various classes [37–39]. Finally, the work briefly discusses the possible

value of the necrotic genotype as a model system for setting up theoretical guidance for monitoring the phytosanitary status of the plant.

2. Materials and Methods

2.1. Tomato Material

IGSV line (breeding code V20368) produces tomato plants with necrotic leaf spots mimicking disease lesions [36]. Plants have indeterminate growth and produce slightly flattened globular fruits. To have a healthy reference for the characterization of leaf symptoms, the F1 hybrid Elisir (Olter) has been identified as a comparison genotype.

A second mutant line was used during foliar analysis via microspectrometry (see below). This line (SA410) was an F_3 progeny deriving from a cross between the necrotic mutant and a mutant line of the *lutescent* (*l*) gene. This gene causes early and gradual degradation of chlorophyll in all parts of the plant, conferring a pale green-yellow colouration to the leaves and a light red colour to the fruit at ripening [40]. The line SA410 was monitored during the first phases of VIS/NIR analysis (see below).

2.2. Growth Conditions

For each line, eighteen plants at the 4–5th true leaf stage were transplanted in three rows (six plants per row) considered to be replicates in open field. To favour the visual inspection of the plants, we left 150 cm between rows and 50 cm between plants along the row. The indeterminate growth of the plants required the use of tutors. To promote the vigour of the fruiting branches and limit their vegetative growth, lateral shoots were removed at weekly intervals during plant growth (Figure 1).

Figure 1. Plants of F1 Elisir (**A**) and IGSV (**B**) during growth and a particular of the Elisir (**C**) and IGSV (**D**) leaves.

The transplant occurred during the second decade of May 2021 at the experimental field of the CREA Research Centre for Engineering and Agro-Food Processing, Monterotondo, Italy (42°05′56.86″ N, 12°37′26.23″ E). For at least three years, the soil was fertilised with cow manure and no chemicals were used for the control of any pathogen or pest.

Plants were drip irrigated with lines placed near the plants. Water supply was scheduled according to the Integrated Production Regulations for processing tomato [41].

2.3. Morphological Characterization of the Autonecrotic Mutant

Before starting the measurements, three representative plants were tagged within each row of the tomato lines, and they were used as samples for the characterization. From 45 days after transplant (DAT) until 74 DAT, we registered the following weekly: the plant height, the chlorophyll content, the height of the necroses in the IGSV line, the order number of the composed leaf of IGSV showing necrotic symptoms. Chlorophyll content was measured on at least three leaflets of the composed leaf in the apical position. The reading was made with a SPAD-502 chlorophyll meter (Minolta Inc., Osaka, Japan) at time intervals corresponding to the plant height measurement.

In the first decade of July, when the maximum temperature and the daily irradiation were at peak, the necrotic symptomatology showed its characteristic expression. For a detailed analysis of the distribution of the autonecrosis along the IGSV plant and within

the leaf, we selected three plants of each genotype inside one row. Three portions of plant were identified: basal, where all the leaves showed severe necroses; median, with necroses not completely diffuse and leaves partially damaged; apical, where the leaves did not show any symptoms. The same scheme was applied for the Elisir's leaves.

From each portion of the three plants, a composed leaf was detached, placed in nylon transparent bags, brought to the laboratory, and photographed. The composed leaves (eighteen in total, nine leaves per genotypes) were weighted via a precision balance Kern (Balingen, Germany) mod. KB 10000-1N (d = 0.1 g) and left to dry at ambient condition until reaching the constant weight. Then, the leaves were weighted again to calculate the dry matter of the composed leaf and the single leaflets.

The photographs were analysed through the ImageJ software, version 1.53k (https://imagej.nih.gov/ij/download.html, accessed 10 November 2023) to determine the total green leaf area and the necrotic (where present) area of the Elisir and IGSV basal, median, and apical leaf. Such values were used to calculate the specific leaf area (mg mm^{-2} leaf area), applying the equation [42]:

$$\text{Specific leaf area}(\text{Specific LA}) = \frac{\text{Leaf area }(\text{cm}^2)}{\text{Leaf dry weight }(g_{DW})}$$

2.4. VIS/NIR Analysis of the Leaves

At the time of transplanting, the plantlets had asymptomatic green leaves. As temperatures and sunlight increased during the first month of growth, the IGSV plants began to progressively develop leaf necrosis starting from the basal leaves. To analyse the autonecrotic behaviour, the leaves of the necrotic IGSV line, the mutant line SA 410, and the healthy hybrid were monitored with a proximal sensor adaptable to field monitoring systems via consecutive readings.

The necrosis began to be visible approximately one month after transplanting. When the plants were at the stage of 5th and 12th true leaf, the VIS/NIR monitoring was applied to the apical green leaf of Elisir, IGSV, and SA410. To this aim, we used the portable and low-cost VIS/NIR spectrometer SCIO^{TM} (Consumer Physics, Tel Aviv, Israel), covering a spectral range between 740 and 1070 nm [37]. On both the 5th and 12th true leaves, three leaflets (the imparipinnate and the two leaflets below) from three plants of each genotype were considered. Three readings were taken on each leaflet.

At the stage of 20th true leaf (67 DAT), IGSV plants showed the typical distribution of the autonecrosis in three areas (basal, median, apical), as described previously. Each area was examined on three plants of Elisir and three plants of IGSV, applying the same operating method of the previous stages. In total, 162 tomato plant samples (81 for the Elisir cultivar and 81 for the IGSV cultivar) were analysed with the VIS/NIR spectrometer to distinguish diseased plants (IGSV) from healthy plants (Elisir control cultivar). For each sample, scans were acquired for each of the three zones considered (basal, medial, and apical). For each zone, 27 spectral scans were performed. The scans were performed through the SCIO spectrometer, which allows scans to be recorded and processed in real-time through the "SCIO Lab" application. The latter stores the data in the cloud to be later exported via a CSV file for analysis. Thanks to the smartphone application, it is possible to use this instrument directly in the field without having to use a PC. A summary of monitoring with the VIS/NIR microspectrometer is reported in Table 2 and shown in Figure 2.

Table 2. Synopsis of the VIS/NIR analysis.

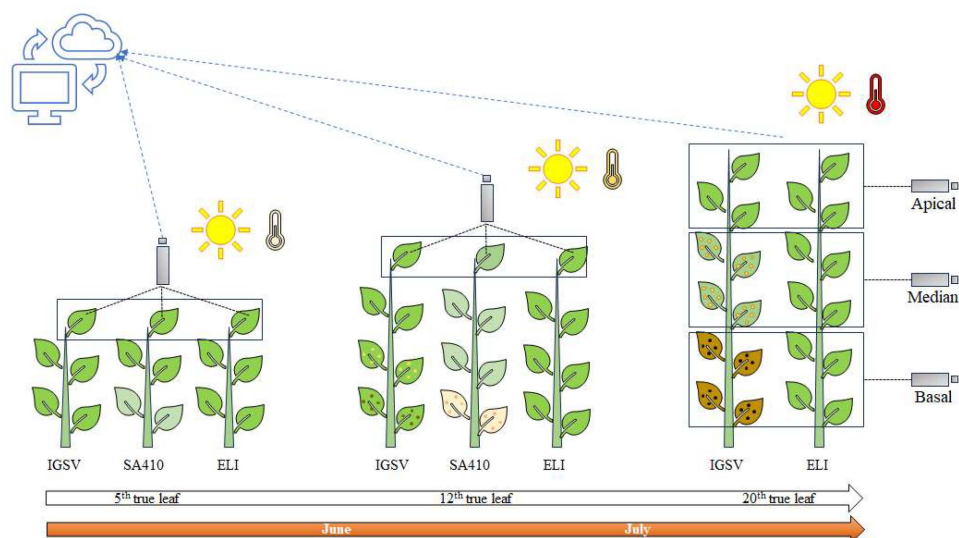| True Leaf	Date of Analysis	DAT *	Leaf Position	Genotype
5th	10 June	27	Apical	Elisir, IGSV, SA410
12th	25 June	42	Apical	Elisir, IGSV, SA410
20th	20 July	67	Basal, median, apical	Elisir, IGSV

* Day After Transplant.

Figure 2. Schematic representation of the methodology adopted for collecting data with the spectrometer SCIO^TM (Consumer Physics, Tel Aviv, Israel).

2.5. Statistical Analysis

The data of plant height, chlorophyll content, and leaf traits were checked for normality and then subjected to the analysis of variance (one-way and two-way) with the PAST software [43], version 3.22 (2018, Øyvind Hammer, University of Oslo, Norway, https://www.nhm.uio.no/english/research/resources/past/, 10 November 2023). Significantly different means were separated via Tuckey's HSD test. Principal Component Analysis (PCA) [44] was performed using the same software to visualise the differences between the genotypes related to the leaf traits.

SIMCA (soft independent modelling by class analogy) statistical analysis was used to analyse 162 samples of tomato plants (81 plants belonging to the Elisir variety and 81 plants belonging to the IGSV line). For each sample, three zones (basal, medial, and apical) were distinguished for a total of 27 scans for each part considered. Considering that the healthy is the only one clearly distinguishable by the pathologist, a single class-modelling approach has been used to distinguish healthy (Elisir) from diseased (IGSV) plants. Apical and median Elisir samples were used to train the SIMCA single-class model. SIMCA was used because, with respect to the two classes considered (healthy and disease), it was attributable with certainty to belong to the healthy class only. For this reason, a class-modelling technique was chosen that allows only one class to be modelled, and for everything else, the further away from the class itself, the more it may happen that the healthy is in the disease or the disease is in the healthy. The analysis was performed using V-Parvus 2010 software and represents a set of PCA models (NIPALS algorithm), one for each class in the dataset (one model in this case), after a separate category autoscale. SIMCA performed a cross-validation of the PCA model of each class (training set) by dividing the data (evaluation set) into 3 contiguous groups (cross-validation groups). The efficiency was evaluated through the classification (training set) and prediction (evaluation set) matrices, which report the percentage of correct classification for each class considered. SIMCA also expressed statistical parameters indicating modelling efficiency (e.g., sensitivity, modelling power for each variable). SIMCA quadratic distances were linearised by converting mean and maximum values to a logarithmic scale and then translating them by adding a value to have all positive values [37,45]. The 54 samples classified as "healthy plants" (apical and median Elisir samples) were divided into an 80% (training set; 43 samples) and a 20% internal evaluation set (11 samples). The partitioning of the artificial datasets was chosen optimally with Euclidean distances, based on Kennard and Stone's algorithm [46] that selects items without a priori knowledge of a regression model. The remaining 108 samples were considered to be external tests. The final output of SIMCA is the linearised

SIMCA distance squared, considered as a metric scale. Samples with a squared linearised SIMCA distance less than the critical distance obtained from the single-class model can be considered "healthy plants," while those with values above the critical distance can be considered "diseased plants". The modelling power of each variable was expressed, representing the influence of that variable in defining the model [47].

3. Results

3.1. Morphological Characterization of the Autonecrotic Mutant

During the plant growth, the rainfall was consistent with the average for central Italy and the maximum temperatures were also normal, being above 30 °C from June to September (Figure 3). The detailed analysis of maximum temperatures and average irradiance showed an increment until the first decade of July for irradiance and between the end of July and mid-August for maximum temperatures (Figure 4). This trend is representative of the area and determined the ideal conditions for the triggering of widespread necrotic manifestation.
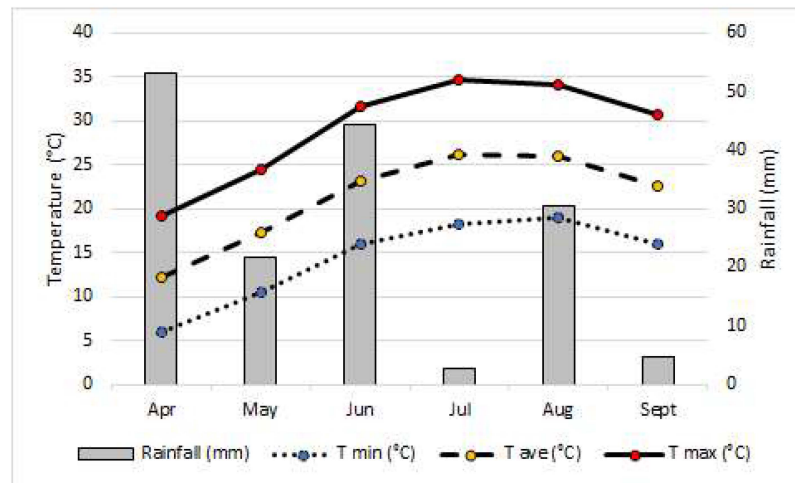

Figure 3. Minimum, average, and maximum temperatures and monthly rainfall registered in the period April–September 2021. Data collected by the Arsial control unit of Monterotondo (RM), location: Grotta Marozza (92 m asl) (https://www.siarl-lazio.it/E1_2.asp, accessed 16 November 2023).
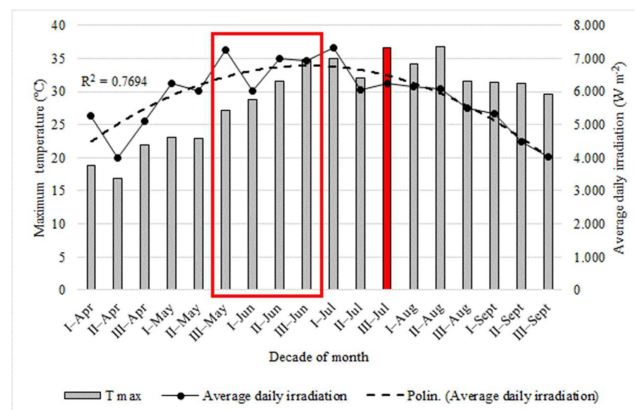

Figure 4. Maximum temperatures (bars) and average daily irradiation (solid line) registered per decade in the period April–September 2021. The dotted line represents the interpolation of the average daily irradiation data. Data collected by the Arsial control unit of Monterotondo (RM), location: Grotta Marozza (92 m asl) (https://www.siarl-lazio.it/E1_2.asp, accessed 16 November 2022). The red square indicates the period from transplant to the first appearance of necrotic specks. The red bar indicates the period when the leaves were collected.

At transplanting (4–5th true-leaf stage), the seedlings of all genotypes had asymptomatic green leaves. Around one month later, leaf necrosis appeared, starting from the basal leaves of the IGSV plants. The development of necrosis occurred as temperatures and solar irradiance gradually increased during the first month of growth (Figure 4). The acropetal progression of the autonecrosis was fully evident in the first decade of July when the three symptomatic zones were visible on each IGSV plant: basal, where all the leaves showed severe necroses; median, with necroses not completely diffuse and leaves partially damaged; and apical, where the leaves did not show any symptoms (Figure 5). As the autonecrosis proceeded, the severity of the symptom led to the complete desiccation of the leaves, starting with the basal ones and then affecting the median and (only partially in a few cases) the apical leaves.
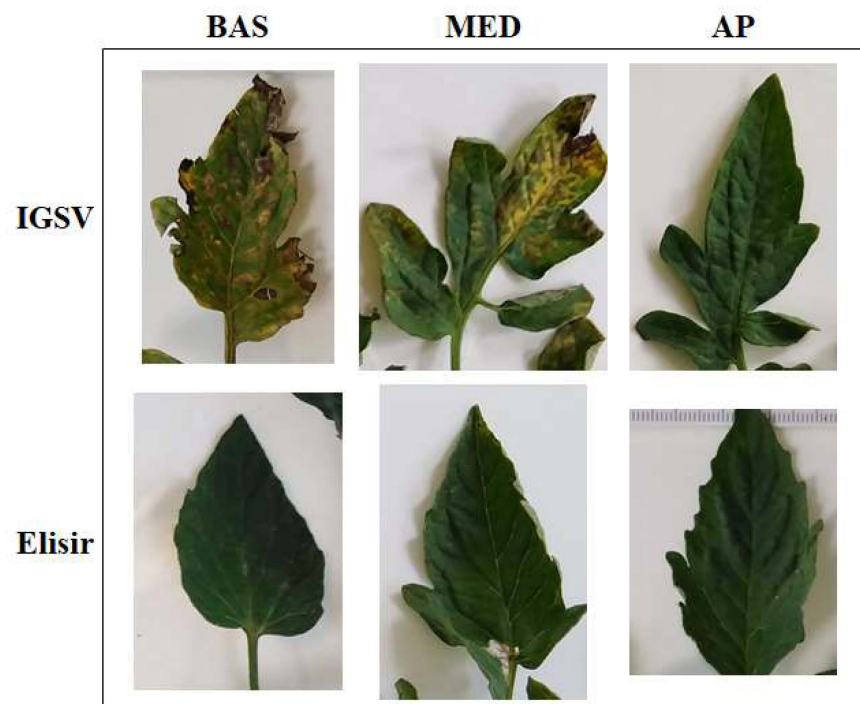

Figure 5. Phenotype of the basal, median, and apical leaflets of IGSV and Elisir F1 at 45 DAT.

The autonecrosis evolved following the plant growth (Figure 6). At 45 DAT, it was visible from the first to the eleventh leaf, while at 75 DAT, the symptoms had reached the twenty-second leaf. The extent of the damage was associated with the acropetal progression. In the basal leaves, the evolution of autonecrosis led the first necrotic spots to enlarge, clump together, and coalesce, turning to a dark brown colour. In some cases, the leaf became completely necrotic. Consequently, the number of spots present on the surface of the basal leaves and their extent was much higher than on the median leaves (Figure 7). In the latter, the mechanism working on the basal leaves was at the beginning, so that the number and size of necrosis were lower (Figure 7). No spots were present on the younger apical leaves where the action of increasing temperatures and irradiance had not yet reached the threshold triggering the autonecroses.
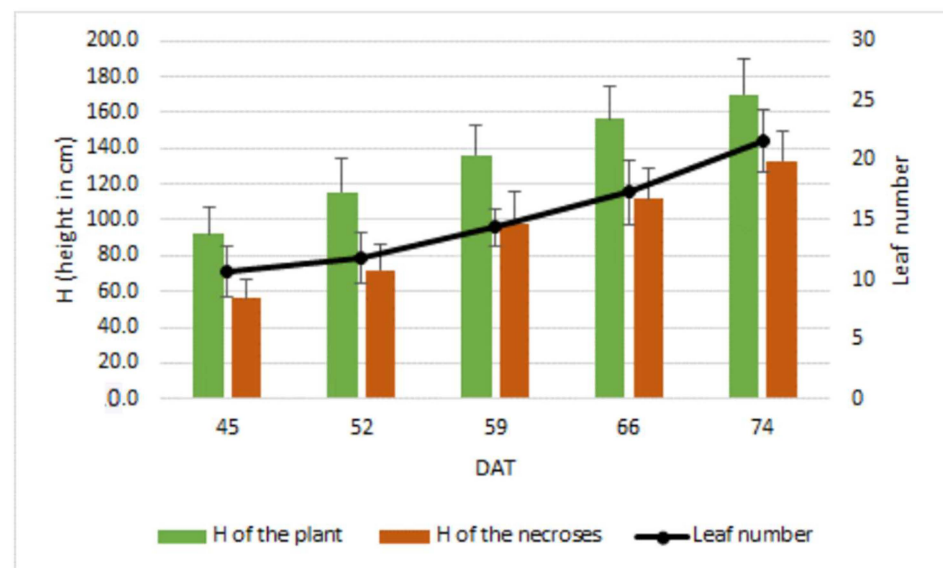
Figure 6. Evolution of autonecroses in the IGSV plants during one month after transplant. The figure reports the height (H) of the plants, the height (H) of the necroses in the plants, and the highest leaf number displaying the necroses (mean ± SD); DAT: Day After Transplant.
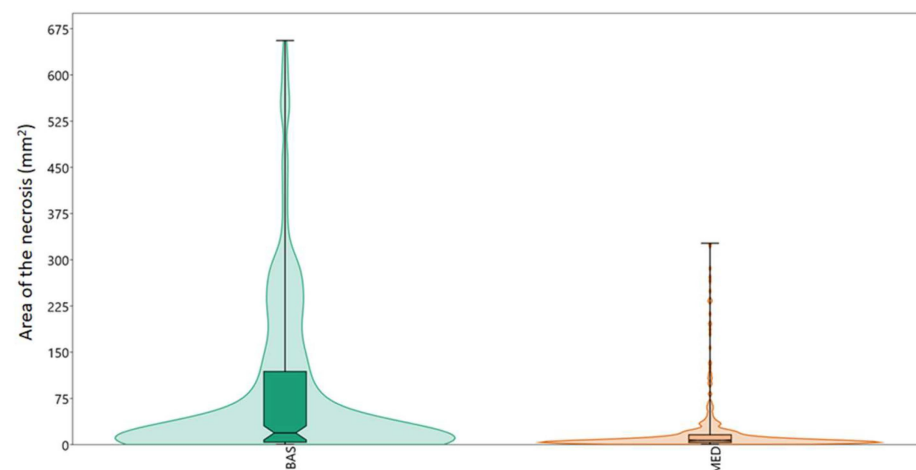

Figure 7. Violin and bar diagram showing the distribution and the amount of the necroses in terms of foliar area (mm^2) in the basal (BAS) and median leaves (MED) of the IGSV plants (67 DAT). The horizontal line inside the box represents the median.

After 67 DAT, when the expression of the autonecrotic phenomenon was at its maximum, the extent of the photosynthesizing green area and the leaf dry matter were statistically higher for the control than the mutant (Table 3). The basal and median leaves of IGSV showed a statistically significant reduction in chlorophyll content compared with the control. In contrast, the level of chlorophyll in the apical leaves of Elisir and IGSV was comparable, as confirmed by a visual check (Figure 5). Obviously, in the mutant, the extent of the necrotic area prevailed, and it accounted for 34% (basal leaves) and 14% (median leaves) of the leaf tissue at the time of the survey. The data also showed that, for both genotypes, the leaves in the median position had a greater weight than the basal leaves (toward a progressive senescence phase) and the apical leaves (still developing and not yet fully active), thus indicating the intermediate area of the plant to be the physiologically most active.

Table 3. Averages of the leaf traits at 67 DAT. Values within columns followed by the different letter are statistically different at the level of $p \leq 0.05$ according to Tuckey's HSD test.

Leaf	Genotype	Chlorophyll (Spad Unit)	Dry Matter (%)	Leaf Weight (g$_{DW}$)	Green LA * (cm^{-2})	LA	
						Necrotic (%)	Specific (cm^2 g^{-1}$_{DW}$)
Basal	IGSV	27.0 c	16.97 b	1.83	109.03	34.17	60.49 b
	Elisir	56.6 a	15.86 b	2.58	218.13	0.45	86.16 a
Median	IGSV	43.5 b	14.17 c	2.22	193.42	14.11	87.18 a
	Elisir	56.4 a	18.05 a	3.74	275.21	0.00	76.14 a
Apical	IGSV	55.5 a	14.90 c	0.61	61.96	0.00	101.68 a
	Elisir	54.8 a	18.16 a	1.19	86.96	0.00	72.04 b

* LA: Leaf area.

The analysis of Specific LA highlighted the effect of the autonecrotic phenomenon. In the control, the Specific LA decreased moving from basal to apical leaves, whereas in IGSV, the trend was the opposite, leading to the lack of a statistical difference between the apical (green) leaves of Elisir and the basal (necrotic) leaves of IGSV. The comparison of leaf traits between the mutant and the control genotype revealed the peculiarity of the former (Figure 8). The first two components of PCA explain more than 80 percent of the existing variability at the leaf level, highlighted by the opposite position of the vectors relating to necrotic leaf area (shifted toward IGSV) and chlorophyll content (close to Elisir).
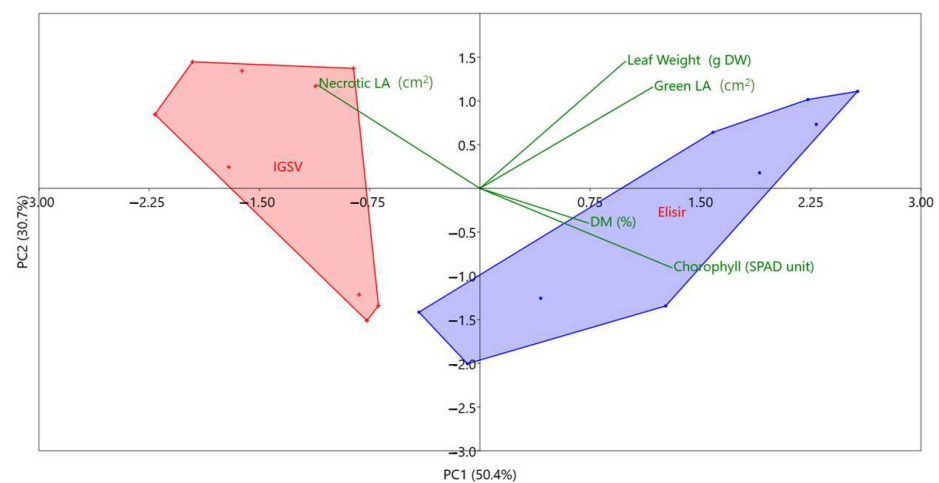

Figure 8. Biplot showing the PCA results of IGSV (pink polygon) and Elisir (violet polygon) separation based on the main foliar traits.

3.2. VIS/NIR Analysis of the Leaves

At the 5th true-leaf stage (27 DAT), all leaves were green, and neither of the two mutants (IGSV and SA410) showed necrotic symptoms on the basal leaves. VIS/NIR analysis limited to the apical leaves alone showed a higher position of the control curve than the two mutants, with a substantially similar trend (Figure 9a). The positioning of the curves did not change at 45 DAT at the 12th true-leaf stage (Figure 9b). At this stage, however, the reflectance values were higher than the previous, especially for the control. This caused a flattening of the curves observed in the second reading. As described previously, the apical leaves were phenotypically similar in the mutants and the control. Thus, the lower reflectance in the mutants could be a signal of physiological activity that will lead to the necrotic manifestation.
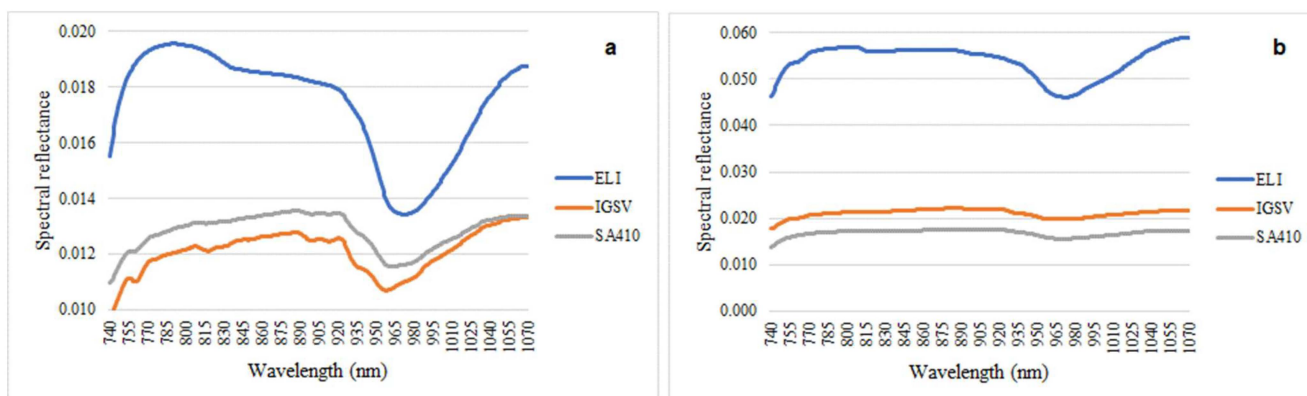
Figure 9. Average curves of spectral reflectance of apical leaf at the stage of 5th (**a**) and 12fth (**b**) true-leaf in control (Elisir) and mutant lines (IGSV and SA410).

As described previously, approximately two months (67 days) after transplanting (20th true-leaf stage), when the autonecrotic process had its maximum expression, it was possible to identify three areas in the plant: in the basal, all the leaves showed severe necrosis, up to complete desiccation; in the median area, the leaves showed yellowish and necrotic sectors; in the last apical portion, the leaves were green.

At this stage, the leaves of the three areas were subjected to VIS/NIR analysis. In general, basal and median leaves of the mutant had a lower spectral reflectance than the control (Figure 10). In both cases, the reflectance of the median, partially damaged, leaves was always higher than the basal level leaves' reflectance, showing a greater degree of damage. It is important to notice the high reflectance gap between the levels of the control plants and IGSV plants. The apical leaves for both genotypes showed a lower curve than the damaged leaves with comparable spectral reflectance levels.
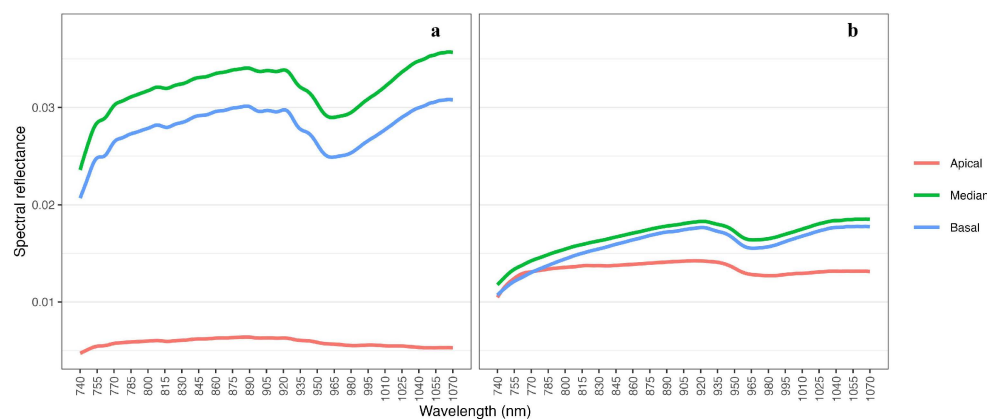

Figure 10. Average curves of spectral reflectance of basal, median, and apical leaves of the control (**a**) and the IGSV mutant (**b**). Analysis at the stage of 20th true leaf (67 DAT).

Figure 11 shows the SIMCA model applied to the dataset of 54 apical and median leaves' Elisir samples and applied to the remaining 108 leaves' samples (162 total samples). The SIMCA logarithmic translational critical distance obtained from the model was 1.95. This figure identifies the boundary between the healthy and unhealthy plants. Only the control plant (Elisir) and the apical leaves of IGSV were represented with values below the critical distance. This means that values below the critical distance are included in the model of healthy plants, while those above the critical distance (i.e., rejected by the model as being healthy) indicate diseased plants, and the more the distance increases above the critical distance, the less healthy the plants are. Table 4 shows the number of tomato plant samples accepted by the model. The sensitivity of the model is 72.09%. The model

recognises almost all the apical leaves of Elisir (n. 24 or 88.9%), rejecting only three. Median and basal leaves are also accepted (n. 18 and n. 15 again for the cultivar Elisir, i.e., 66.7% and 55.6%) as well as the IGSV apical (n. 22 i.e., 81.5%) for which only five were rejected. The proportion of accepted was the lowest for the median (29.6%) and basal (33.4%) leaves of IGSV. In both the training and testing phases, the leaves of Elisir were almost all accepted by the model (except for three); the leaves of IGSV were also accepted, although in the latter, the percentage of diseased was higher than in Elisir.
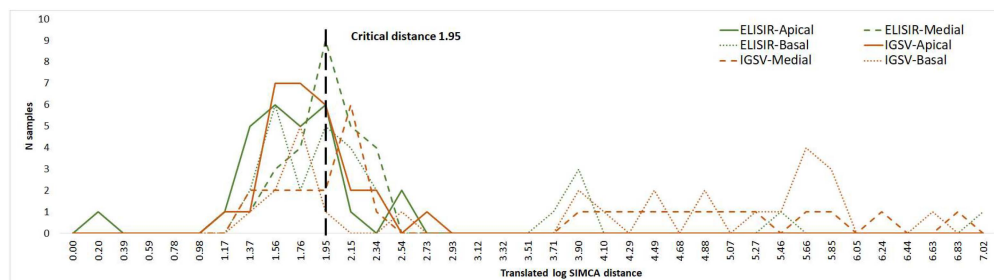

Figure 11. Soft independent modelling by class analogy histogram by frequency class of the SIMCA translational log square performed on the spectral dataset and tested on the mean values for each tomato sample, considering two classes ("healthy leaves_Elisir and IGSV_apical leaves", "damaged leaves_IGSV" and "defective sample"). The dashed black line represents the critical value (i.e., the model boundary).

Table 4. Number of samples accepted by the SIMCA model as healthy plants; numbers of samples included within the SIMCA model.

Cultivar	Leaf	N. Accepted	N. Rejected	Accepted (%)
ELISIR	Apical	24	3	88.9
	Median	18	9	66.7
	Basal	15	12	55.6
IGSV	Apical	22	5	81.5
	Median	8	19	29.6
	Basal	9	18	33.4

Figure 12 shows the modelling power of the SIMCA model applied to the VIS/NIR spectral bands, indicating which bands made a greater contribution to the identification of healthy plants. Although all spectral bands contributed excellently to the model, as shown in Figure 12, it is evident that the values with the greatest modelling power are those between 860–870 nm and those between 1050 and 1060 nm.
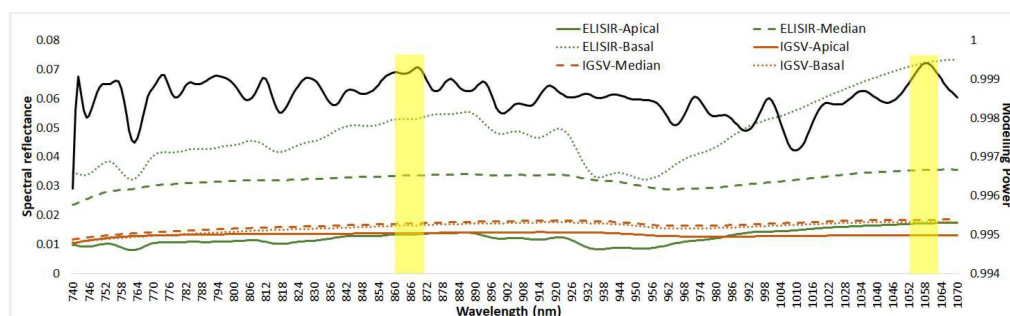

Figure 12. Modelling power obtained by the SIMCA model used to assess healthy plants. The yellow box highlights the most important spectral range that distinguished between healthy plants and sick plants.

4. Discussion

Observations on the morphological characteristics have confirmed that the *Rcr3^{lyc}/Cf-2^{pim}* gene combination of the IGSV (breeding code V20368) genotype was able to trigger the necrotic expression. This interaction is referred to as hybrid necrosis, a common type of hybrid incompatibility in plants, as defined by [12]. The IGSV autonecrotic tomato line spontaneously developed necrotic lesions in the acropetal direction from the 5–6th true leaf stage in response to the natural increase in air temperature and light irradiation, which are the usual conditions during tomato cultivation. As observed by [36,48], the *Rcr3^{lyc}/Cf-2^{pim}* combination caused, at the biochemical level, the activation of ATPases and antioxidant enzymes (catalases and peroxidases). Increased ATPase activity (also present in the plant–pathogen interaction) was observed in the central and basal leaves as an early event before the triggering of the oxidative burst. Correspondingly, the antioxidant enzymes were higher in the basal leaves, where the oxidative burst leading to cell necrosis was active. A similar interaction has been studied for lettuce and cotton. In interspecific lettuce hybrids between *Lactuca sativa* and *Lactuca saligna*, a temperature-dependent autoimmunity reaction leads to necrotic lesions. In this case, the lowering of the temperature triggered the formation of necrosis [49]. Interspecific F$_1$ plants of *Gossipium barbadense* × *G. hirsutum* showed necrotic (red) spots in leaves and infertile flowers [50]. The development of the spots resembled that observed for IGSV: the number of spots and size of the necrosis increased and became more severe in the oldest leaves. In addition, the chlorophyll content was significantly reduced in the necrotic leaves compared with the normal leaves (as reported in the present study), while the ROS production and the peroxidase activity were higher in the necrotic plants. In the IGSV line, the phenomenon is so intense that, in the older basal leaves, the necrotic area covered more than one third of the tissue. Overall, the results confirmed the genuine nature of IGSV's hybrid necrosis, characterising its formation pattern and placing it within a group of genotypes spread across a wide range of species.

Yu et al. [51] observed in pepper a chlorophyll loss from apical to basal leaves because of the pigment degradation in the older leaves. The data of Elisir did not confirm such behaviour; at a visual check, the plants appeared to still be in full growth and did not show any trace of senescence. Considering the growth stage, this does not exclude the possibility that some ageing processes were in progress, primarily in the basal leaves. On the other side, the autonecrosis greatly reduced the chlorophyll content from apical green to basal damaged leaves, thus resembling the process described by [51]. However, the chlorophyll decrease was mainly due to the autonecrotic process that masked the leaf senescence. Yao et al. [26] observed a decline in SPAD values in wheat leaves challenged by stripe rust starting from 2 to 13 days after inoculation. Chlorophyll also played a role in determining the values of Specific LA (SLA). This is an important variable in growth models, as it relates dry matter production to light interception and photosynthesis and can vary during the plant's development [52,53]. The increase in light intensity modifies acclimation-related traits such as the leaf thickness, which increases, and the SLA, which decreases. Both are morpho-physiological tools aimed at protecting the plant from high irradiance [42,54]. In our work, such a mechanism was confirmed for the control Elisir because the apical leaves that were more exposed to light had a SLA lower than the median and basal leaves, which were in a more sun-sheltered position. Autonecrosis constitutes the phenotypic manifestation of biochemical events occurring at the cellular level at an earlier asymptomatic stage [3]. Already in apical green leaves, it is possible to assume there has been damage to the photosynthetic system and a reduction in the biomass per unit area, leading to high SLA in the IGSV genotype. In [42], it is stated that the difficulty of quickly dissipating the excess of light energy can cause photoinhibition and damage to the photosynthetic reaction centre. This can reduce the maximization of carbon gain per unit leaf mass, resulting in a low leaf weight and high SLA. Median and basal leaves were older and developed a larger leaf area, although they had a different percentage of necrotic tissue. In this case, the photosynthetic structures that remained concentrated in stricter green areas because of tissue destruction were able to increase the leaf weight, reducing the SLA.

Beyond the interest in studies of genetics, physiology, and evolutionary processes, the autonecrotic genotype can have scientific value for the application of a smart system for monitoring biotic and abiotic stresses. Indeed, autoimmune interactions and lesion mimic mutants activate the same biochemical mechanisms (hypersensitive response, systemic resistance mediated by salicylic acid, reactive oxygen species, ethylene, induction of programmed cell death) associated with responses to environmental stresses, including pathogen attack [12,13,15,55,56]. References discussing the genetics of hybrid necrosis and LMM as well as their usefulness for evolutionary studies are largely available, while the practical application of their peculiarity is rarer. In our case, the idea was to assess whether and to what extent the use of the genetically altered genotype (hybrid necrosis) compatible with normal growth can be a model and can have value for applications in the proximal sensing of biotic and abiotic stress.

Relevant studies [21,23,57,58] underlined as helpful can be the use of hyperspectral data for monitoring the physiological changes occurring when a plant is challenged by a pathogen. At the biochemical level, plant diseases alter the leaf internal structure and chemical composition of the tissues, giving a new and specific spectral signature at different growth stages. This is true particularly for those pathogens causing necrotic lesions [16]. Thus, hyperspectral tools coupled with proximal sensing can help the farmers detect a pathogen better than traditional methods and act quickly by reducing inoculum, damage, and the amount of pesticide distributed. Zhang et al. [24], analysing tomato fields infected by *Phytophtora infestans* in California by means of a spectrometer, observed that the spectrum of healthy plants in the near infrared (NIR) was higher than the diseased ones. The same pattern was confirmed by [59] for tomato leaves inoculated with *Alternaria solani* and *P. infestans*. Such a pattern corresponds to the analysis we made with SCIO on apical (Figure 9) or median and basal leaves (Figure 10). As mentioned previously, the display of autonecrosis in the basal and median leaves is just the final expression of biochemical events occurring at an earlier asymptomatic stage, possibly already in the apical leaves. Moreover, comparing the basal and median leaves of the control with those of IGSV, the NIR spectra of the former remained higher than that of the mutant, and the spectrum of the basal (highly damaged) leaves was lower than the median. IGSV reflectance at the basal and median levels was lower than in Elisir. In the former, the autonecrosis caused structural changes in the leaf tissue which led the necrotic effect to become predominant on any senescence effect and equalised the spectrum of differently positioned leaves.

The application of the SIMCA multivariate analysis allowed for the identification of the critical distance and the boundary between healthy and damaged leaves. In general, the model showed good efficiency in discriminating the type of leaf, successfully including in the healthy samples the majority of Elisir leaves and the apical green leaves of IGSV (sensitivity equal to 72.09%). Interestingly, in the SIMCA model, the percentage of accepted samples in the control decreased from younger (apical) to older (basal) leaves, thus indicating a possible capacity of the model in pointing out a senescence effect. In this case, it was interesting to apply SIMCA because the leaves that visibly exhibited a distinguishable feature were only the healthy ones, and therefore an approach had to be used that allowed only one class to be used for classification. In other cases, other more traditional techniques can be used as a classification system (PLSDA, LDA; [60]) or more complex systems based on nonlinear classification techniques (ANN; [61]). The model identified the wavelengths between 860–870 nm or between 1050–1060 nm as having the greatest modelling power. The ranges fall within those identified by [24] for tomato infected by *P. infestans* in California fields. The spectra in the interval 750–930 nm allowed for the discrimination of the best five severity groups (including healthy plants), followed by the intervals 950–1030 and 1040–1130. In his spectral analysis [59] observed the largest difference between the leaves of healthy tomato plants and plants infected with *P. infestans* or *A. solani* between 750 and 1000 nm as a consequence of the collapse of leaf cell structure.

However, results confirmed that our model individuate a stricter interval in the same ranges able to discriminate the healthy from infected plants. We agree with [59] about

the potential of hyperspectral imaging in identifying some diseases on tomato leaves. A key point that our study reveals is the chance of detecting the tissue alteration before the appearance of visible symptoms. The practical implications lead to the use of such spectral sensors in precision agriculture where, as outlined by [17], can find an advantageous application in proximal sensor platform. As stated by [24] timely and precise detecting and monitoring of the infected plants of tomato by mapping the disease at the field level through hyperspectral images can help the farmers for a wiser use of pesticides with positive effects on pollution and the economic return of cultivation.

Moreover, but not least, the detection of disease severity by hyperspectral imaging at the leaf, single plant, and canopy scale can have a role phenotyping application [23,57]. From this point of view, the use of isogenic lines, i.e., lines that differ genetically only in the gene of interest, would be particularly important. An example is the RIG and RIM tomato lines studied by [36] which differ only in the presence or absence of the resistance gene to the bacterium *Pseudomonas syringae* pv. *tomato* present in a small region of chromosome 5 and introgressed from *L. pimpinellifolium*. The use of such lines would make it possible to isolate only the effects of the phenomenon studied, thus avoiding all the 'background noise'. The use of mutants with alterations in the machinery devoted to defence responses such as the one described in this paper or, in any case, in systems of tolerance to biotic and abiotic stresses can also be highly informative within the application of advanced sensor systems such as bioristors [62,63] or wearables and portable sensors [64,65] for monitoring morphological, physiological, and biochemical parameters in response to environmental alterations.

Mutants for autoimmunity or hybrid necrosis could be a precious tool for digital applications in agriculture. The mutant studied in the present work has further elements of interest associate to specific features. First of all, the defence mechanisms elicited by the autonecrotic manifestation are those common in the plant-pathogen interaction in tomato and other species, thus representing and providing a study model. The autonecrosis has a high grade of repeatability because it is triggered by summer weather conditions once the threshold of temperature and irradiance are exceeded. Although mimicking a plant-pathogen interaction, it does not need artificial inoculations in controlled environment, the symptomatic manifestation is uniform avoiding eventual temporal and spatial variability that can occur in the field. In their work [24], Zhang et al. needed to localise tomato fields containing late blight diseased plants with various severities, distributed in strips.

Importantly, the physiological, phenotypic, and instrumental monitoring of symptomatology can be performed in open-field conditions i.e., the level where sensor for precision agriculture must operate. Hybrid necrosis is common and phenotypically similar in many different species belonging to different taxa and controlled by alleles that can be recessive or dominant [13]. Given the botanical proximity to other Solanaceae, most of the information sprouting from tomato can be extended in exploring the response of other vegetables to pathogen attack.

In a visionary perspective, such type of mutants can be used as "emitters" of volatile organic compounds (VOCs) able to activate defence systems in neighbouring plants. Two recent works in different species as tea [66] and *Arabidopsis* [67] confirmed as the release of plants VOCs related to the herbivore- or pathogen-challenged plants was a mechanism for triggering damaged-associated biochemical pathways [68]. Genotypes such as that of the present work can be a useful tool to prove the efficacy of VOCs release from the whole plant, whether and how the VOCs are received by neighbours and if the activation of plant defence is realistic in open field conditions.

5. Conclusions

The hybrid necrosis of the IGSV line showed the predicted phenological pattern, and a link between symptomatology and hyperspectral reflectance was highlighted, with the 860–870 nm and 1050–1060 nm wavelengths having the greatest modelling power. The lower-than-normal reflectance values of the apparently healthy leaves (the apical ones)

of the necrotic plant indicate that, although phenotypically not visible, the activation of autonecrosis was in progress. Repeated studies on mutants of the type described may find useful application in the development of predictive models for early detection of pathogens (or other stresses) in tomato by proximal sensing. It is possible to imagine an extension of the studied model to other species of the same family (Solanaceae) and beyond.

Since many mechanisms underlying the physiological response to pathogens are similar, the modelling of the mutant appears extensible to a wider variety of cases. Similar mutants sensitive to abiotic stresses could constitute additional biological tools that could increase the range of environmental stresses that can be analysed, as well as facilitate the understanding of plant-environment interaction and the development of ground-based monitoring systems.

Author Contributions: Conceptualization, E.S.; methodology, E.S. and C.B.; validation, C.C., S.V. and M.B.; formal analysis, E.S., C.C. and S.V.; investigation, E.S., A.D.G. and C.B.; resources, S.F.; data curation, E.S., C.C., S.V. and M.B.; writing—original draft preparation, E.S., M.B. and C.B.; writing—review and editing, E.S., M.B. and S.B.; visualization, S.B.; supervision, E.S. All authors have read and agreed to the published version of the manuscript.

Institutional Review Board Statement: Not applicable.

Data Availability Statement: The data presented in this study are available on request from the corresponding author.

Conflicts of Interest: The authors declare no conflict of interest.

References

1. Dangl, J.L.; Dietrich, R.A.; Richberg, M.H. death don't have no mercy: Cell death programs in plant-microbe interactions. *Plant Cell* **1996**, *8*, 1793–1807. [CrossRef]
2. Hammond-Kosack, K.E.; Jones, J.D. Resistance gene-dependent plant defense responses. *Plant Cell* **1996**, *8*, 1773–1791. [CrossRef]
3. Lamb, C.; Dixon, R.A. The oxidative burst in plant disease resistance. *Annu. Rev. Plant Physiol. Plant Mol. Biol.* **1997**, *48*, 251–275. [CrossRef]
4. Beltran, P.M.J.; Federspiel, J.D.; Sheng, X.; Cristea, I.M. Proteomics and integrative omic approaches for understanding host–pathogen interactions and infectious diseases. *Mol. Syst. Biol.* **2017**, *13*, 922. [CrossRef]
5. Peyraud, R.; Dubiella, U.; Barbacci, A.; Genin, S.; Raffaele, S.; Roby, D. Advances on plant–pathogen interactions from molecular toward systems biology perspectives. *Plant J.* **2017**, *90*, 720–737. [CrossRef]
6. Jones, J.; Dangl, J. The plant immune system. *Nature* **2006**, *444*, 323–329. [CrossRef]
7. Dangl, J.L.; Horvath, D.M.; Staskawicz, B.J. Pivoting the plant immune system from dissection to deployment. *Science* **2013**, *341*, 746–751. [CrossRef]
8. Dixon, M.S.; Golstein, C.; Thomas, C.M.; van der Biezen, E.A.; Jones, J.D.G. Genetic complexity of pathogen perception by plants: The example of *Rcr3*, a tomato gene required specifically by *Cf-2*. *Proc. Natl. Acad. Sci. USA* **2000**, *97*, 8807–8814. [CrossRef]
9. Rooney, H.C.; Van't Klooster, J.W.; van der Hoorn, R.A.; Joosten, M.H.; Jones, J.D.; de Wit, P.J. Cladosporium Avr2 Inhibits Tomato Rcr3 Protease Required for Cf-2-Dependent Disease Resistance. *Science* **2005**, *308*, 1783–1786. [CrossRef] [PubMed]
10. Kourelis, J.; Malik, S.; Mattinson, O.; Krauter, S.; Kahlon, P.S.; Paulus, J.K.; van der Hoorn, R.A.L. Evolution of a guarded decoy protease and its receptor in solanaceous plants. *Nat. Commun.* **2020**, *11*, 4393. [CrossRef] [PubMed]
11. Krüger, J.; Thomas, C.M.; Golstein, C.; Dixon, M.S.; Smoker, M.; Tang, S.; Mulder, L.; Jones, J.D. A tomato cysteine protease required for Cf-2-dependent disease resistance and suppression of autonecrosis. *Science* **2002**, *296*, 744–747. [CrossRef]
12. Wan, W.; Kim, S.; Castel, B.; Charoennit, N.; Chae, E. Genetics of autoimmunity in plants: An evolutionary genetics perspective. *New Phytol.* **2021**, *229*, 1215–1233. [CrossRef] [PubMed]
13. Bomblies, K.; Weigel, D. Hybrid necrosis: Autoimmunity as a potential gene-flow barrier in plant species. *Nat. Rev. Genet.* **2007**, *8*, 382–393. [CrossRef]

14. Moeder, W.; Yoshioka, K. Lesion mimic mutants. *Plant Signal. Behav.* **2008**, *3*, 764–767. [CrossRef] [PubMed]

15. Bruggeman, Q.; Raynaud, C.; Benhamed, M.; Delarue, M. To die or not to die? Lessons from lesion mimic mutants. *Front. Plant Sci.* **2015**, *6*, 24. [CrossRef] [PubMed]

16. Mahlein, A.-K. Plant disease detection by imaging sensors—Parallels and specific demands for precision agriculture and plant phenotyping. *Plant Dis.* **2016**, *100*, 241–251. [CrossRef]

17. Pallottino, F.; Antonucci, F.; Costa, C.; Bisaglia, C.; Figorilli, S.; Menesatti, P. Optoelectronic proximal sensing vehicle-mounted technologies in precision agriculture: A review Partial Least Squares Regression. *Comput. Electron. Agric.* **2019**, *162*, 859–873. [CrossRef]

18. Pane, C.; Manganiello, G.; Nicastro, N.; Ortenzi, L.; Pallottino, F.; Cardi, T.; Costa, C. Machine learning applied to canopy hyperspectral image data to support biological control of soil-borne fungal diseases in baby leaf vegetables. *Biol. Control* **2021**, *164*, 104784. [CrossRef]

19. Navarro, A.; Nicastro, N.; Costa, C.; Pentangelo, A.; Cardarelli, M.; Ortenzi, L.; Pallottino, F.; Cardi, T.; Pane, C. Sorting biotic and abiotic stresses on wild rocket by leaf-image hyperspectral data mining with an artificial intelligence model. *Plant Methods* **2022**, *18*, 45. [CrossRef]

20. Violino, S.; Figorilli, S.; Ferrigno, M.; Manganiello, V.; Pallottino, F.; Costa, C.; Menesatti, P. A data-driven bibliometric review on precision irrigation. *Smart Agric. Technol.* **2023**, *5*, 100320. [CrossRef]

21. Mahlein, A.-K.; Kuska, M.; Behmann, J.; Polder, G.; Walter, A. Hyperspectral sensors and imaging technologies in phytopathology: State of the art. *Annu. Rev. Phytopathol.* **2018**, *56*, 535–558. [CrossRef]

22. Martinelli, F.; Scalenghe, R.; Davino, S.; Panno, S.; Scuderi, G.; Ruisi, P.; Villa, P.; Stroppiana, D.; Boschetti, M.; Goulart, R.L.; et al. Advanced methods of plant disease detection: A review. *Agron. Sustain. Dev.* **2015**, *35*, 1–25. [CrossRef]

23. Thomas, S.; Kuska, M.T.; Bohnenkamp, D.; Brugger, A.; Alisaac, E.; Wahabzada, M.; Behmann, J.; Mahlein, A.-K. Benefits of hyperspectral imaging for plant disease detection and plant protection: A technical perspective. *J. Plant Dis. Prot.* **2018**, *125*, 5–20. [CrossRef]

24. Zhang, M.; Qin, Z.; Liu, X.; Ustin, S.L. Detection of stress in tomatoes induced by late blight disease in California, USA, using hyperspectral remote sensing. *Int. J. Appl. Earth Obs. Geoinf.* **2003**, *4*, 295–310. [CrossRef]

25. Oerke, E.-C.; Herzog, K.; Toepfer, R. Hyperspectral phenotyping of the reaction of grapevine genotypes to *Plasmopara viticola*. *J. Exp. Bot.* **2016**, *67*, 5529–5543. [CrossRef]

26. Yao, Z.; Lei, Y.; He, D. Early visual detection of wheat stripe rust using visible/near-infrared hyperspectral imaging. *Sensors* **2019**, *19*, 952. [CrossRef] [PubMed]

27. Hou, B.; Hu, Y.; Zhang, P.; Hou, L. Potato Late Blight Severity and Epidemic Period Prediction Based on Vis/NIR Spectroscopy. *Agriculture* **2022**, *12*, 897. [CrossRef]

28. Huang, Y.; Wang, D.; Liu, Y.; Zhou, H.; Sun, Y. Measurement of early disease blueberries based on vis/nir hyper-spectral imaging system. *Sensors* **2020**, *20*, 5783. [CrossRef]

29. Jiang, Q.; Wu, G.; Tian, C.; Li, N.; Yang, H.; Bai, Y.; Zhang, B. Hyperspectral imaging for early identification of strawberry leaves diseases with machine learning and spectral fingerprint features. *Infrared Phys. Technol.* **2021**, *118*, 103898. [CrossRef]

30. Li, J.; Huang, W.; Tian, X.; Wang, C.; Fan, S.; Zhao, C. Fast detection and visualization of early decay in citrus using Vis-NIR hyperspectral imaging. *Comput. Electron. Agric.* **2016**, *127*, 582–592. [CrossRef]

31. Chu, X.; Zhang, K.; Wei, H.; Ma, Z.; Fu, H.; Miao, P.; Jiang, H.; Liu, H. A Vis/NIR spectra-based approach for identifying bananas infected with Colletotrichum musae. *Front. Plant Sci.* **2023**, *14*, 1180203. [CrossRef]

32. Bagheri, N.; Mohamadi-Monavar, H. Early detection of fire blight disease of pome fruit trees using visible-nir spec-trometry and dimensionality reduction methods. *J. Agric. Mach.* **2020**, *10*, 37–48.

33. Najjar, K. Sensing Botrytis cinerea in Tomato Using Visible/Near-Infrared (VIS/NIR) Spectroscopy. Ph.D. Dissertation, Palestine Technical University—Kadoorie, Tulkarm, Palestine, 2020.

34. Berardo, N.; Pisacane, V.; Battilani, P.; Scandolara, A.; Pietri, A.; Marocco, A. Rapid detection of kernel rots and mycotoxins in maize by near-infrared reflectance spectroscopy. *J. Agric. Food Chem.* **2005**, *53*, 8128–8134. [CrossRef]

35. Morellos, A.; Tziotzios, G.; Orfanidou, C.; Pantazi, X.E.; Sarantaris, C.; Maliogka, V.; Alexandridis, T.K.; Moshou, D. Non-destructive early detection and quantitative severity stage classification of Tomato Chlorosis Virus (ToCV) infection in young tomato plants using vis–NIR Spectroscopy. *Remote Sens.* **2020**, *12*, 1920. [CrossRef]

36. Santangelo, E.; Fonzo, V.; Astolfi, S.; Zuchi, S.; Caccia, R.; Mosconi, P.; Mazzucato, A.; Soressi, G.P. The Cf-2/Rcr3esc gene interaction in tomato (*Lycopersicon esculentum*) induces autonecrosis and triggers biochemical markers of oxidative burst at cellular level. *Funct. Plant Biol.* **2003**, *30*, 1117–1125. [CrossRef]

37. Violino, S.; Taiti, C.; Marone, E.; Pallottino, F.; Costa, C. A statistical tool to determine the quality of extra virgin olive oil (EVOO). *Eur. Food Res. Technol.* **2022**, *248*, 2825–2832. [CrossRef]

38. Forina, M.; Oliveri, P.; Casale, M.; Lanteri, S. Multivariate range modeling, a new technique for multivariate class modeling: The uncertainty of the estimates of sensitivity and specificity. *Anal. Chim. Acta* **2008**, *622*, 85–93. [CrossRef] [PubMed]

39. Ceccarelli, D.; Antonucci, F.; Costa, C.; Talento, C.; Ciccoritti, R. An artificial class modelling approach to identify the most largely diffused cultivars of sweet cherry (*Prunus avium* L.) in Italy. *Food Chem.* **2020**, *333*, 127515. [CrossRef]

40. Barry, C.S.; Aldridge, G.M.; Herzog, G.; Ma, Q.; McQuinn, R.P.; Hirschberg, J.; Giovannoni, J.J. Altered chloroplast development and delayed fruit ripening caused by mutations in a zinc metalloprotease at the *lutescent2* locus of tomato. *Plant Physiol.* **2012**, *159*, 1086–1098. [CrossRef] [PubMed]

41. Regione Emilia-Romagna. Pomodoro da Industria. Parte Agronomica. 2019. Available online: http://agricoltura.regione.emilia-romagna.it/produzioni-agroalimentari/temi/bio-agro-climambiente/agricoltura-integrata/disciplinari-produzione-integrata-vegetale/Collezione-dpi/2019/orticole-2019 (accessed on 16 November 2023).

42. Fan, X.-X.; Xu, Z.-G.; Liu, X.-Y.; Tang, C.-M.; Wang, L.-W.; Han, X.-L. Effects of light intensity on the growth and leaf development of young tomato plants grown under a combination of red and blue light. *Sci. Hortic.* **2013**, *153*, 50–55. [CrossRef]

43. Hammer, Ø.; Harper, D.A.T.; Ryan, P.D. Past: Paleontological statistics software package for education and data analysis. *Palaeontol. Electron.* **2001**, *4*, 1–9.

44. Montanari, M. *Statistica ambientale. Analisi Multivariata. Metodologie di Ordinamento*; SISSAD Snc: Trieste, Italy, 2012.

45. Zanetti, M.; Costa, C.; Greco, R.; Grigolato, S.; Aalmo, G.O.; Cavalli, R. How wood fuels' quality relates to the standards: A class-modelling approach. *Energies* **2017**, *10*, 1455. [CrossRef]

46. Kennard, R.; Stone, L. Computer aided design of experiments. *Technometrics* **1969**, *11*, 137–148. [CrossRef]

47. Sgarbossa, A.; Costa, C.; Menesatti, P.; Antonucci, F.; Pallottino, F.; Zanetti, M.; Grigolato, S.; Cavalli, R. A multivariate SIMCA index as discriminant in wood pellet quality assessment. *Renew. Energy* **2015**, *76*, 258–263. [CrossRef]

48. De Biasi, M.G.; Astolfi, S.; Acampora, A.; Zuchi, S.; Fonzo, V.; Santangelo, E.; Caccia, R.; Badiani, M.; Soressi, G.P. A H_2O_2-forming peroxidase rather than a NAD(P)H-dependent O2●—Synthase may be the major player in cell death responses controlled by the Pto—Fen complex following fenthion treatment. *Funct. Plant Biol.* **2003**, *30*, 409–417. [CrossRef]

49. Jeuken, M.J.; Zhang, N.W.; McHale, L.K.; Pelgrom, K.; Boer, E.D.; Lindhout, P.; Michelmore, R.W.; Visser, R.G.; Niks, R.E. *Rin4* causes hybrid necrosis and race-specific resistance in an interspecific lettuce hybrid. *Plant Cell* **2009**, *21*, 3368–3378. [CrossRef] [PubMed]

50. Deng, J.; Fang, L.; Zhu, X.; Zhou, B.; Zhang, T. A CC-NBS-LRR gene induces hybrid lethality in cotton. *J. Exp. Bot.* **2019**, *70*, 5145–5156. [CrossRef] [PubMed]

51. Yu, K.-Q.; Zhao, Y.-R.; Zhu, F.-L.; Li, X.-L.; He, Y. Mapping of chlorophyll and SPAD distribution in pepper leaves during leaf senescence using visible and near-infrared hyperspectral imaging. *Trans. ASABE* **2016**, *59*, 13–24. [CrossRef]

52. Rinaldi, M. Variation of Specific Leaf Area for Sugar Beet Depending on Sowing Date and Irrigation. *Ital. J. Agron.* **2003**, *7*, 23–32.

53. Aguirre-Becerra, H.; García-Trejo, J.F.; Vázquez-Hernández, C.; Alvarado, A.M.; Feregrino-Pérez, A.A.; Contreras-Medina, L.M.; Guevara-Gonzalez, R.G. Effect of extended photoperiod with a fixed mixture of light wavelengths on tomato seedlings. *HortScience* **2020**, *55*, 1832–1839. [CrossRef]

54. Evans, J.R.; Poorter, H. Photosynthetic acclimation of plants to growth irradiance: The relative importance of specific leaf area and nitrogen partitioning in maximizing carbon gain. *Plant Cell Environ.* **2001**, *24*, 755–767. [CrossRef]

55. van Esse, H.P.; Klooster, J.W.V.; Bolton, M.D.; Yadeta, K.A.; van Baarlen, P.; Boeren, S.; Vervoort, J.; de Wit, P.J.; Thomma, B.P. The *Cladosporium fulvum* virulence protein Avr2 inhibits host proteases required for basal defense. *Plant Cell* **2008**, *20*, 1948–1963. [CrossRef]

56. Fei, W.; Liu, Y. Biotrophic Fungal Pathogens: A Critical Overview. *Appl. Biochem. Biotechnol.* **2023**, *195*, 1–16. [CrossRef] [PubMed]

57. Wahabzada, M.; Mahlein, A.-K.; Bauckhage, C.; Steiner, U.; Oerke, E.-C.; Kersting, K. Metro maps of plant disease dynamics—Automated mining of differences using hyperspectral images. *PLoS ONE* **2015**, *10*, e0116902. [CrossRef] [PubMed]

58. Lowe, A.; Harrison, N.; French, A.P. Hyperspectral image analysis techniques for the detection and classification of the early onset of plant disease and stress. *Plant Methods* **2017**, *13*, 80. [CrossRef]

59. Xie, C.; Shao, Y.; Li, X.; He, Y. Detection of early blight and late blight diseases on tomato leaves using hyperspectral imaging. *Sci. Rep.* **2015**, *5*, 16564. [CrossRef] [PubMed]

60. Costa, C.; Antonucci, F.; Pallottino, F.; Aguzzi, J.; Sun, D.-W.; Menesatti, P. Shape analysis of agricultural products: A review of recent research advances and potential application to computer vision. *Food Bioprocess Technol.* **2011**, *4*, 673–692. [CrossRef]

61. Violino, S.; Benincasa, C.; Taiti, C.; Ortenzi, L.; Pallottino, F.; Marone, E.; Mancuso, S.; Costa, C. AI-based hyperspectral and VOCs assessment approach to identify adulterated extra virgin olive oil. *Eur. Food Res. Technol.* **2021**, *247*, 1013–1022. [CrossRef]

62. Janni, M.; Cocozza, C.; Birilli, F.; Pignatelli, S.; Vurro, F.; Coppede, N.; Bettelli, M.; Calestani, D.; Loreto, F.; Zappettini, A. Real-time monitoring of Arundo donax response to saline stress through the application of in vivo sensing technology. *Sci. Rep.* **2021**, *11*, 18598. [CrossRef]

63. Janni, M.; Coppede, N.; Bettelli, M.; Briglia, N.; Petrozza, A.; Summerer, S.; Vurro, F.; Danzi, D.; Cellini, F.; Marmiroli, N.; et al. In vivo phenotyping for the early detection of drought stress in tomato. *Plant Phenomics* **2019**, *2019*, 6168209. [CrossRef]

64. Coatsworth, P.; Gonzalez-Macia, L.; Collins, A.S.P.; Bozkurt, T.; Güder, F. Continuous monitoring of chemical signals in plants under stress. *Nat. Rev. Chem.* **2023**, *7*, 7–25. [CrossRef] [PubMed]

65. Presti, D.L.; Di Tocco, J.; Massaroni, C.; Cimini, S.; De Gara, L.; Singh, S.; Raucci, A.; Manganiello, G.; Woo, S.L.; Schena, E.; et al. Current understanding, challenges and perspective on portable systems applied to plant monitoring and precision agriculture. *Biosens. Bioelectron.* **2023**, *222*, 115005. [CrossRef] [PubMed]

66. Chen, S.; Zhang, L.; Cai, X.; Li, X.; Bian, L.; Luo, Z.; Li, Z.; Chen, Z.; Xin, Z. (E)-Nerolidol is a volatile signal that induces defenses against insects and pathogens in tea plants. *Hortic. Res.* **2020**, *7*, 52. [CrossRef] [PubMed]

67.   Aratani, Y.; Uemura, T.; Hagihara, T.; Matsui, K.; Toyota, M. Green leaf volatile sensory calcium transduction in Arabidopsis. *Nat. Commun.* **2023**, *14*, 6236. [CrossRef]
68.   Razo-Belman, R.; Ozuna, C. Volatile Organic Compounds: A Review of Their Current Applications as Pest Biocontrol and Disease Management. *Horticulturae* **2023**, *9*, 441. [CrossRef]